Supplementary Figure. 1

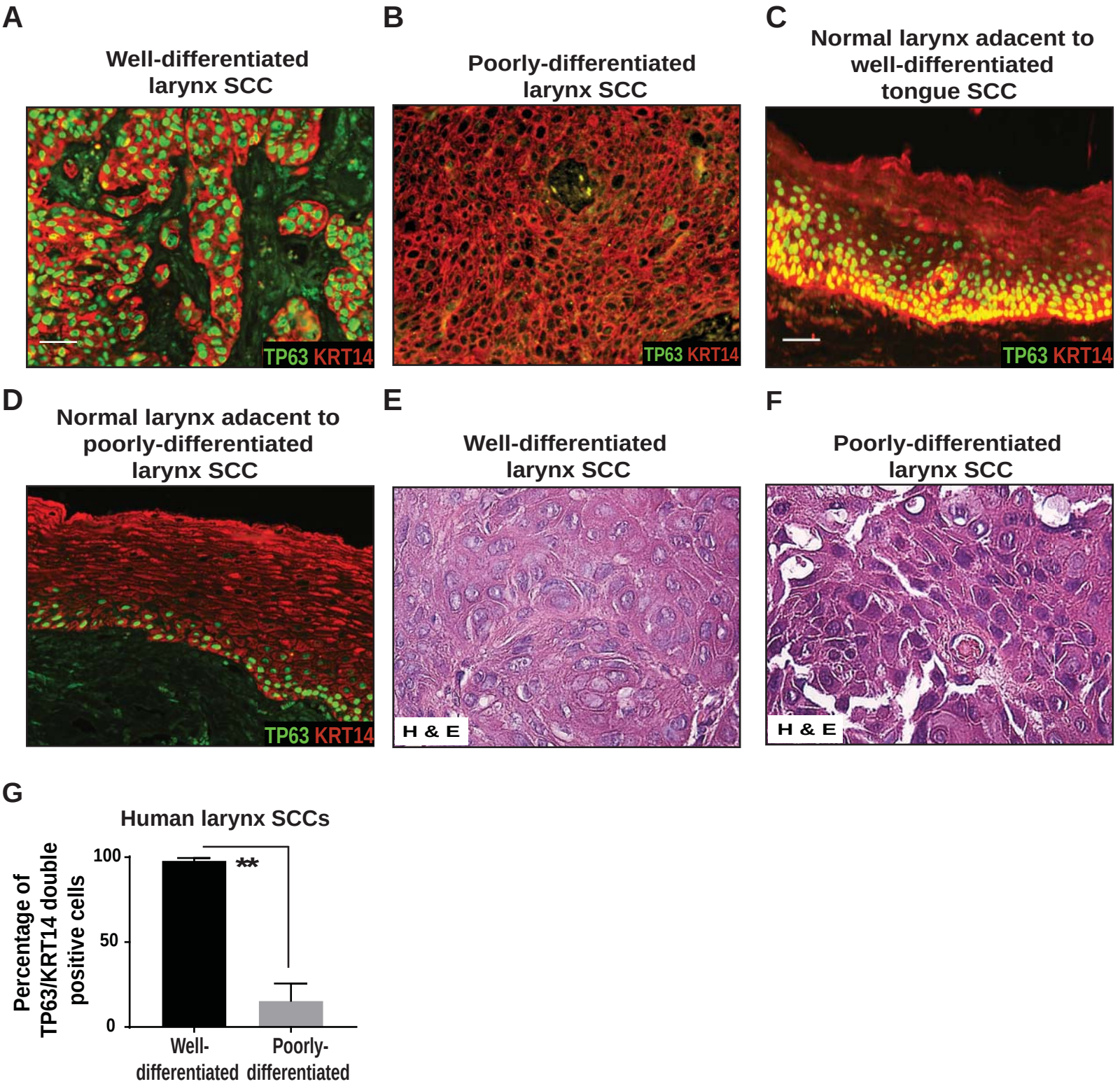

Supplementary Figure 1. TP63 expression is downregulated in late-stage human larynx HNSCCs. (A-D) Immunostaining with antibodies against TP63 (green) and KRT14 (red) on sections of well-differentiated larynx SCC (n=3), poorly-differentiated larynx SCC (n=4), and their corresponding adjacent normal larynx. Scale bars = 50 µm. (E, F) Hematoxylin and eosin staining of well-differentiated larynx SCC and poorly-differentiated larynx SCC. Scale bars = 50 µm. (G) Quantification of TP63/KRT14 double positive cells from A and B (two-tailed unpaired Student *t*-test, **: $P < 0.01$; Mean ± SD).

Supplementary Figure. 2

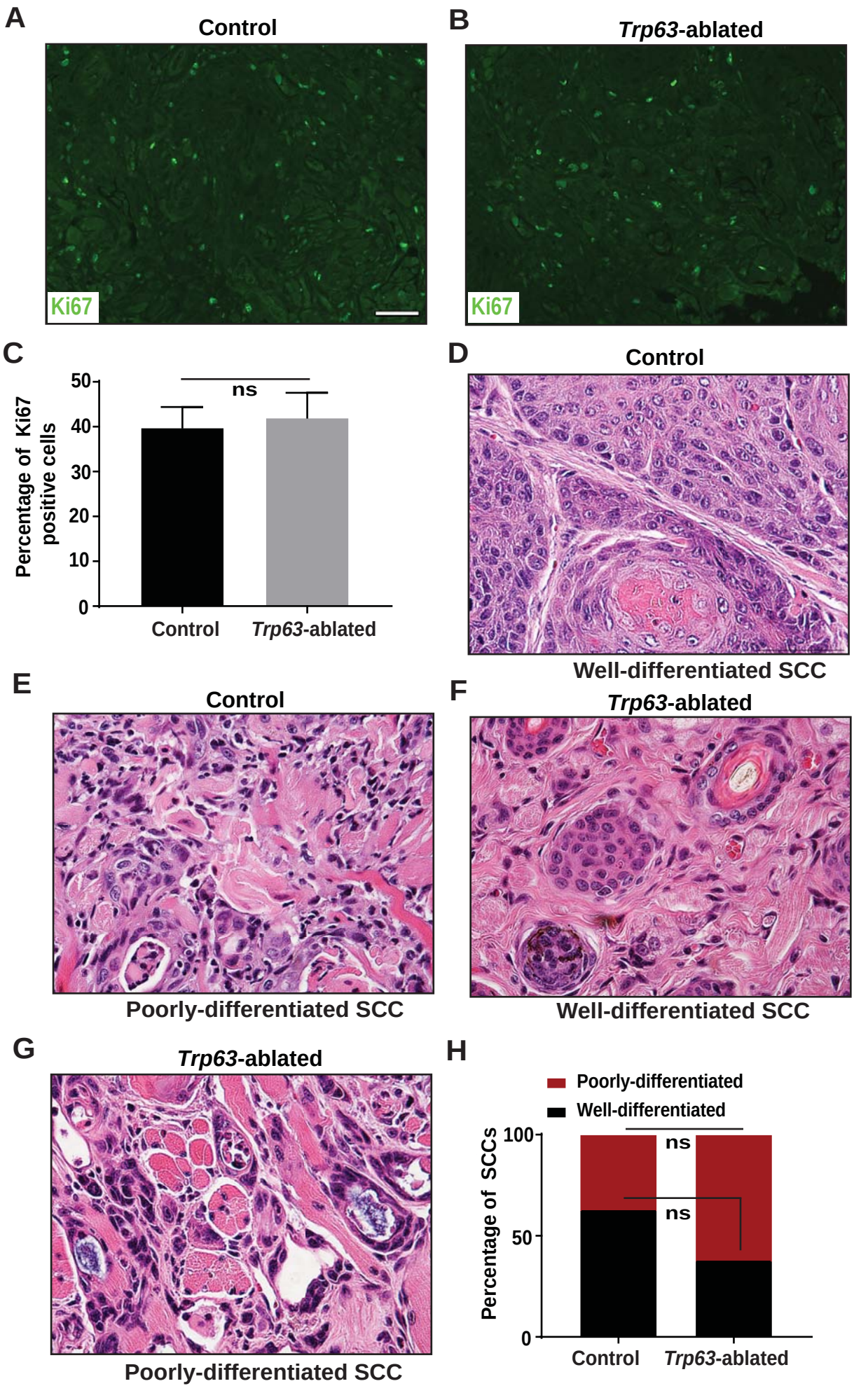

Supplementary Figure 2. Histopathological analysis of mouse tongue SCCs. (A) Immunostaining with antibody against Ki67 on SCCs obtained from control and *Trp63*-ablated mice. (C) Quantification of Ki67 positive cells from A and B (two-tailed unpaired Student *t*-test, “ns” indicates not significant; P > 0.05). (D-G) Hematoxylin and Eosin (H & E) staining of well- and poorly-differentiated oral SCCs obtained from control and *Trp63*-ablated mice at the end of the study. Scale bars = 50 µm. (H) Graph depicting the percentage of well- and poorly-differentiated SCCs obtained from A-D (Fisher’s exact test, “ns” indicates not significant; P= 0.6193).

Supplementary Figure. 3

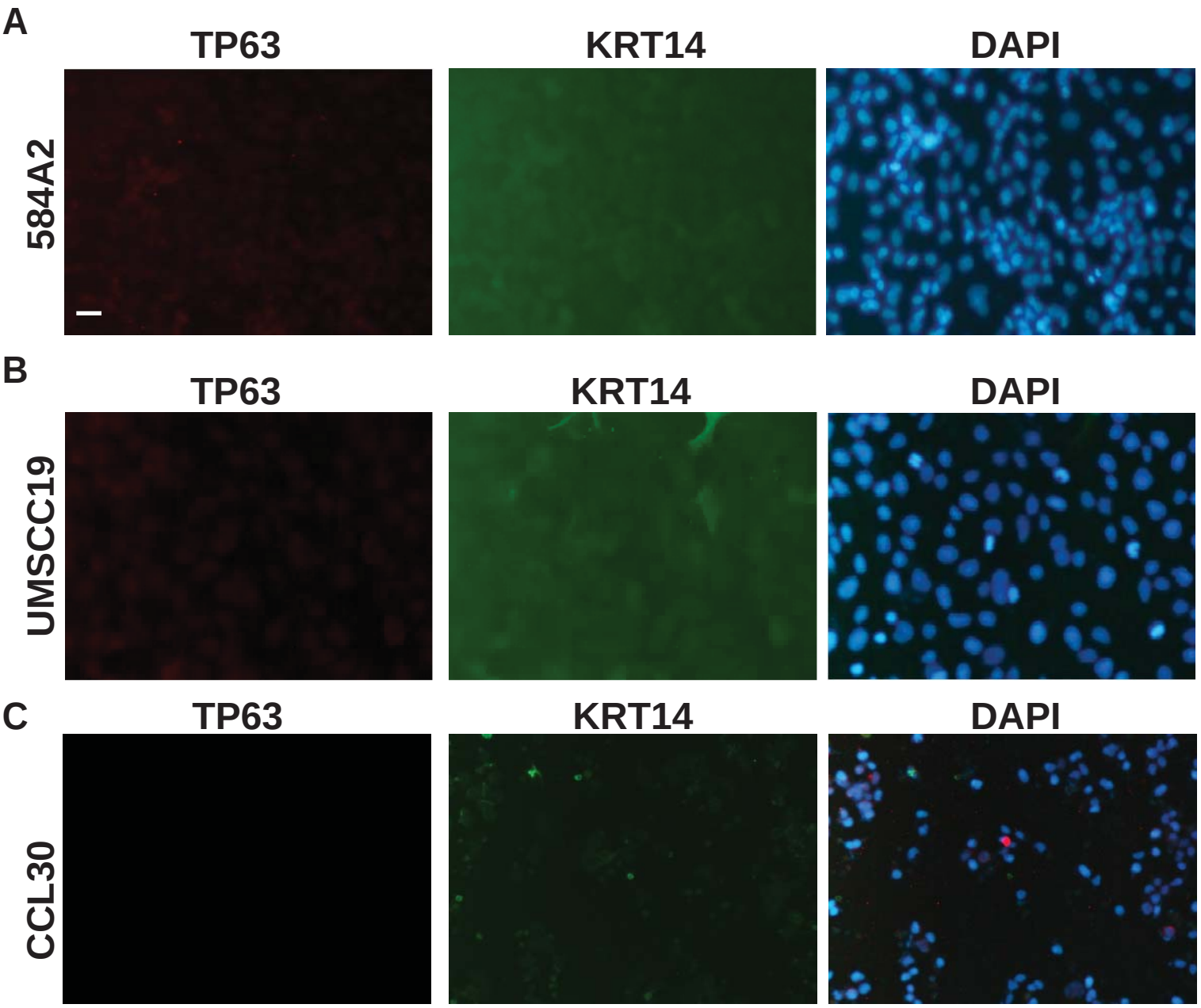

Supplementary Figure 3. TP63 and KRT14 (epithelial marker) expression is lost in a subset of human HNSCC cell lines. (A-C) Immunostaining with antibodies against TP63 (red) (I) and KRT14 (green) (II) and DAPI (III) on SCC cell lines, 584A2, UMSCC19, and CCL30. TP63 immunostaining studies were carried out with p63α antibody. Scale bars = 50 µm.

Supplementary Figure. 4

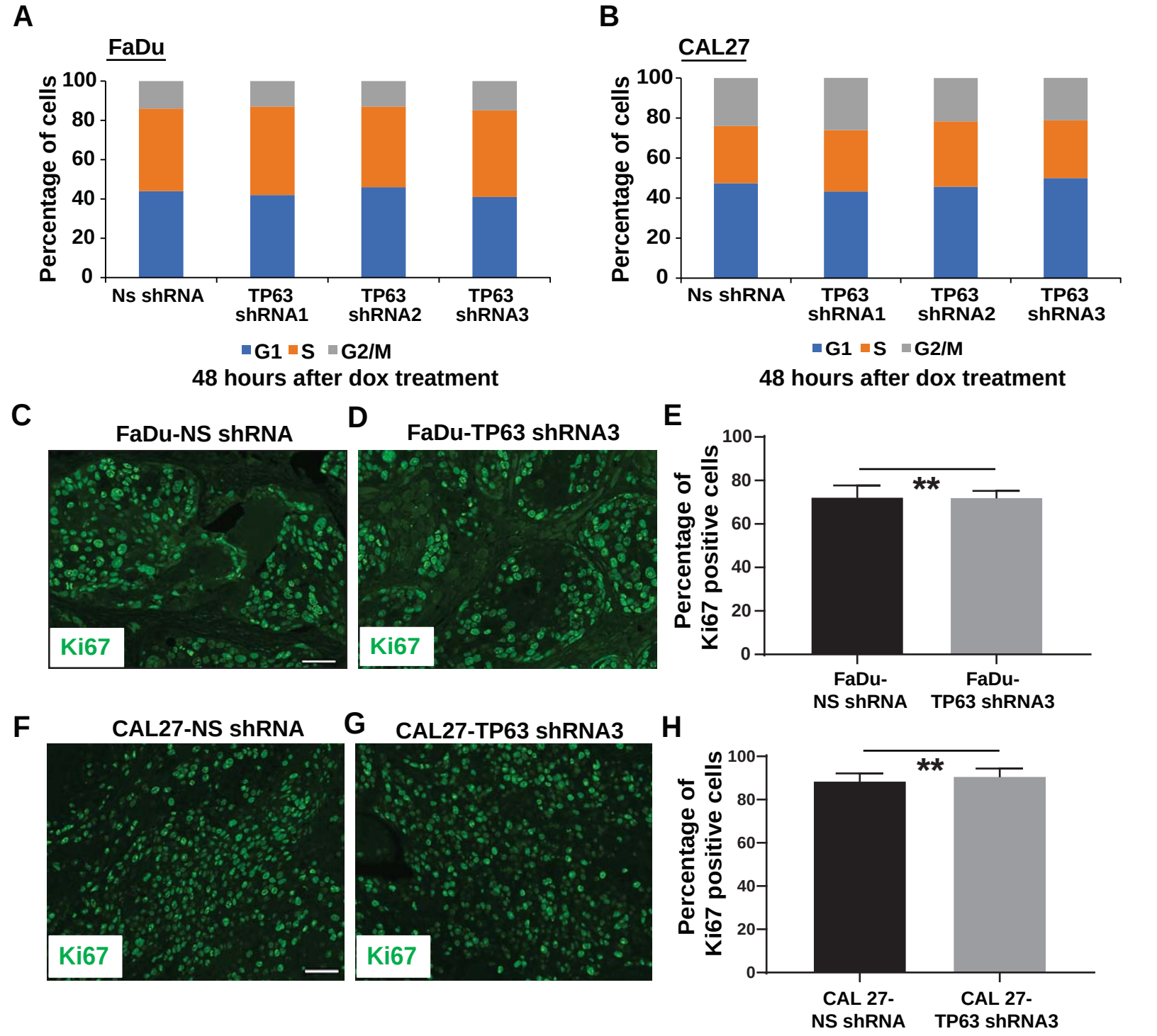

Supplementary Figure 4. Loss of TP63 in HNSCC cell lines does not alter cell cycle distribution. (A, B) The percentage of cells in each phase of cell cycle (G1, S, and G2/M) was assessed using PI staining followed by flow cytometry. (C, D) Immunostaining with antibody against Ki67 on SCCs obtained from mice implanted with either FaDu-NS shRNA or FaDu-TP63 shRNA3 mice. (E) Quantification of Ki67 positive cells from C and D (two-tailed unpaired Student *t*-test, **: $P < 0.01$; Mean ± SD). (F, G) Immunostaining with antibody against Ki67 on SCCs obtained from mice implanted with either CAL27-NS shRNA or CAL27-TP63 shRNA3 cells. (H) Quantification of Ki67 positive cells from F and G (two-tailed unpaired Student *t*-test, “ns” indicates not significant; $P > 0.05$).

Supplementary Figure. 5

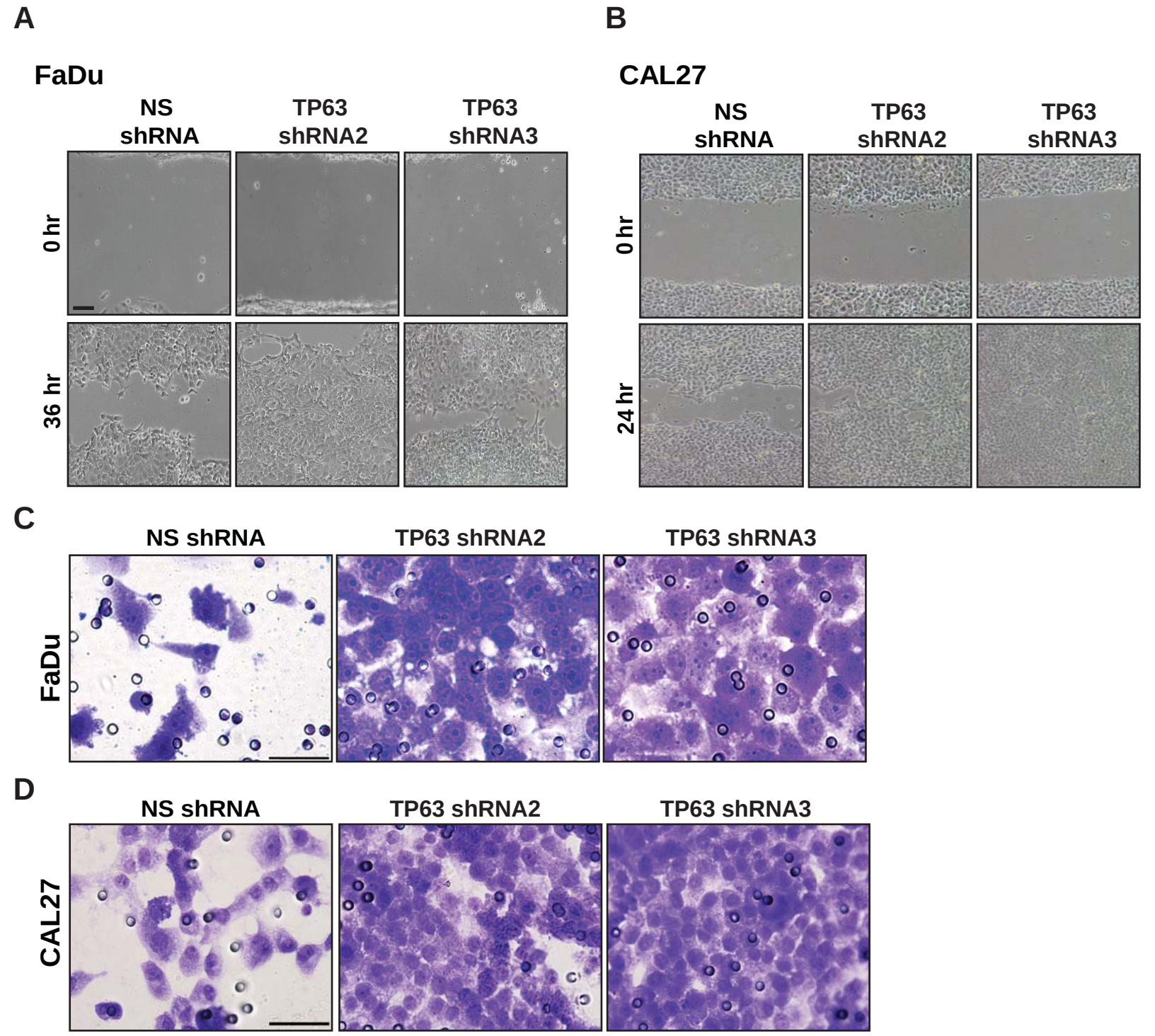

Supplementary Figure 5. Loss of TP63 promotes the migration and invasion of HNSCC cell lines. (A, B) The migratory properties of indicated cell lines were assessed using a scratch assay. Representative images were obtained immediately after scratch (0 hours) and 36 hours post scratch. Scale bars = 50 µm. (C, D) The invasive properties of indicated cell lines was assessed using a matrigel-coated transwell assay. Representative images show the invading cells at the end of experiment (36 hours after seeding on to the matrigel-coated transwell chambers). Scale bars = 50 µm. Results for scratch and invasion assay were obtained from three independent experiments.

Supplementary Figure. 6

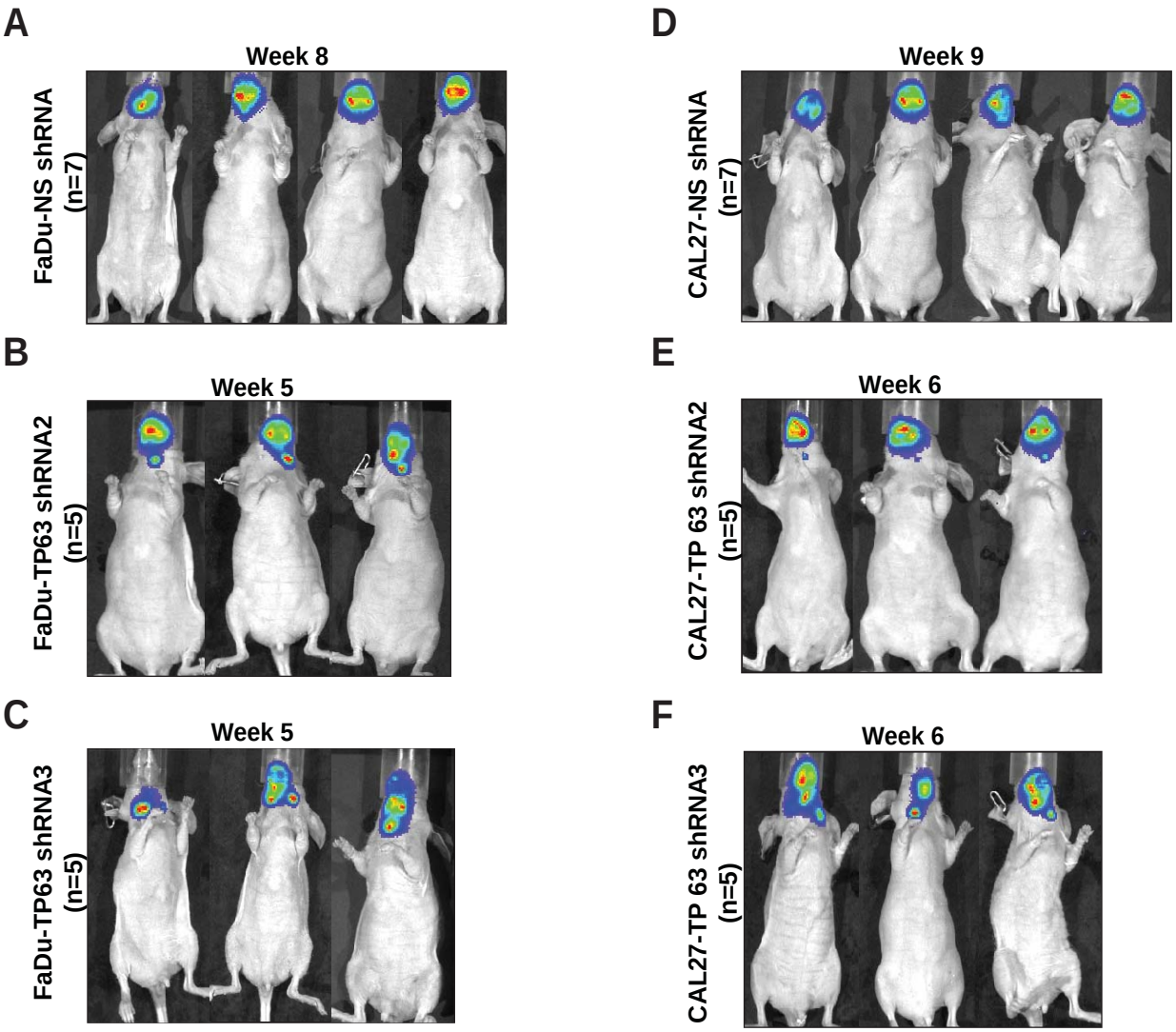

Supplementary Figure 6. Loss of TP63 promotes cervical lymph node metastasis *in vivo*. (A) Bioluminescence imaging (BLI) of mice implanted with FaDu-NS shRNA at week 8. (B, C) BLI of mice implanted with FaDu-TP63 shRNA 2 and FaDu-TP63 shRNA 3 at week 8. (D) BLI of mice implanted with CAL27-NS shRNA at week 9. (E, F) BLI of mice implanted with CAL27- TP63 shRNA 2 and CAL27-TP63 shRNA 3 at week 6.

Supplementary Figure. 7

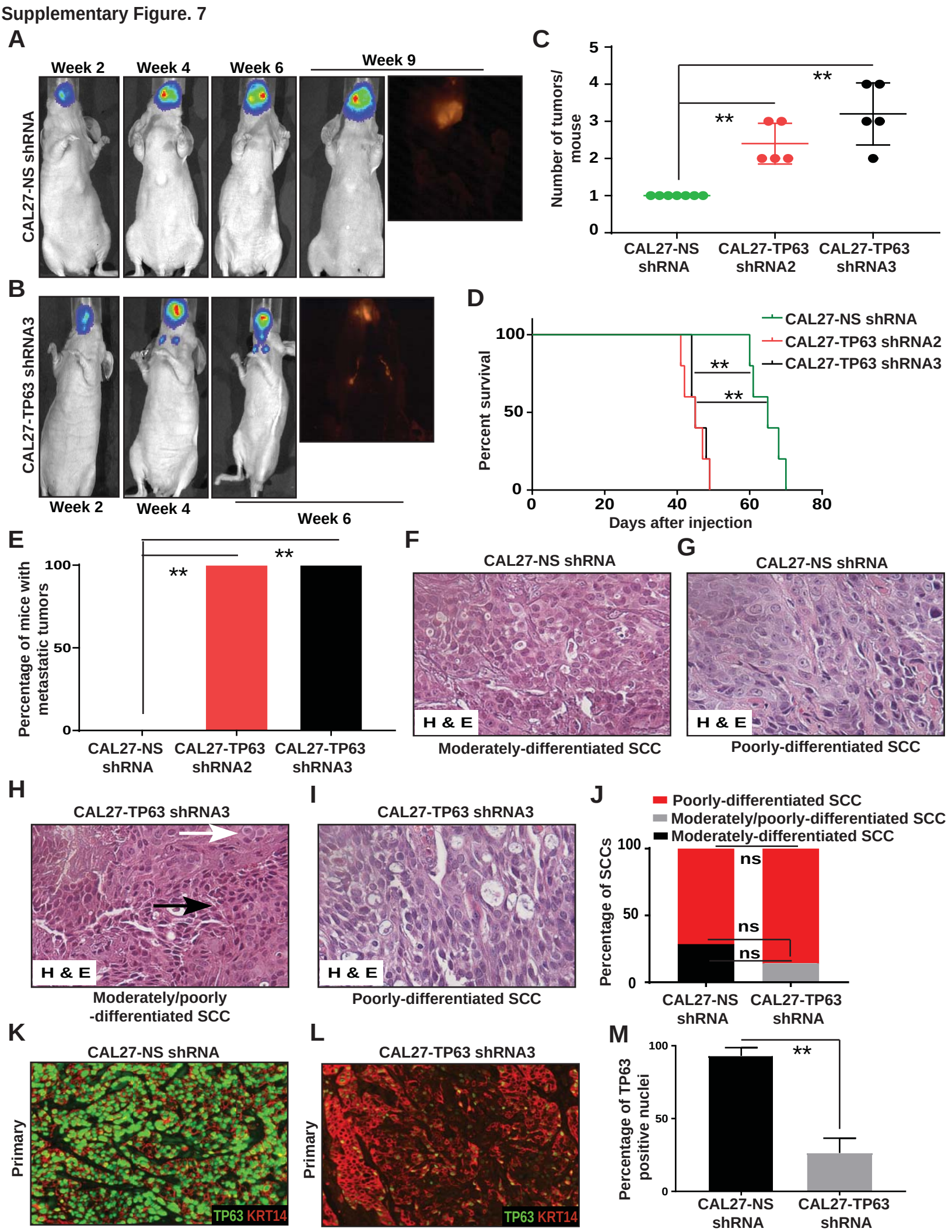

Supplementary Figure 7. Loss of TP63 promotes cervical lymph node metastasis of CAL27 cells. (A, B) *In vivo* bioluminescence imaging of athymic nude mice implanted with CAL27-NS shRNA (n=7) and CAL27-TP63 shRNA3 (n=5) at various time points. (C-E) Graphs depicting the average number of tumors/mouse, (Mann-Whitney *U*-test, **: $P < 0.01$), survival (log-rank test, **: $P < 0.01$), and percentage of mice with metastatic tumors in mice implanted with CAL27-NS shRNA (n=7), CAL27-TP63 shRNA2 (n=5), and TP63 shRNA3 (n=5) at the end of study (Fisher's exact test, **; $P < 0.05$). (F-I) Hematoxylin and eosin staining of moderately, moderately/poorly differentiated, and poorly-differentiated HNSCCs obtained from mice implanted with CAL27-NS shRNA and CAL27-TP63 shRNA3. (J) Graph depicting the percentage of moderately and poorly-differentiated HNSCCs obtained from F-I (Fisher's exact test, "ns" indicates not significant; $P > 0.05$). (K, L) Immunostaining with antibodies against TP63 (red) and KRT14 (green) on HNSCCs obtained from mice implanted with CAL27-NS shRNA and CAL27-TP63 shRNA3. (M) Quantification of TP63 positive nuclei from K and L (two-tailed unpaired Student *t*-test, **: $P < 0.01$; Mean ± SD).

Supplementary Figure. 8

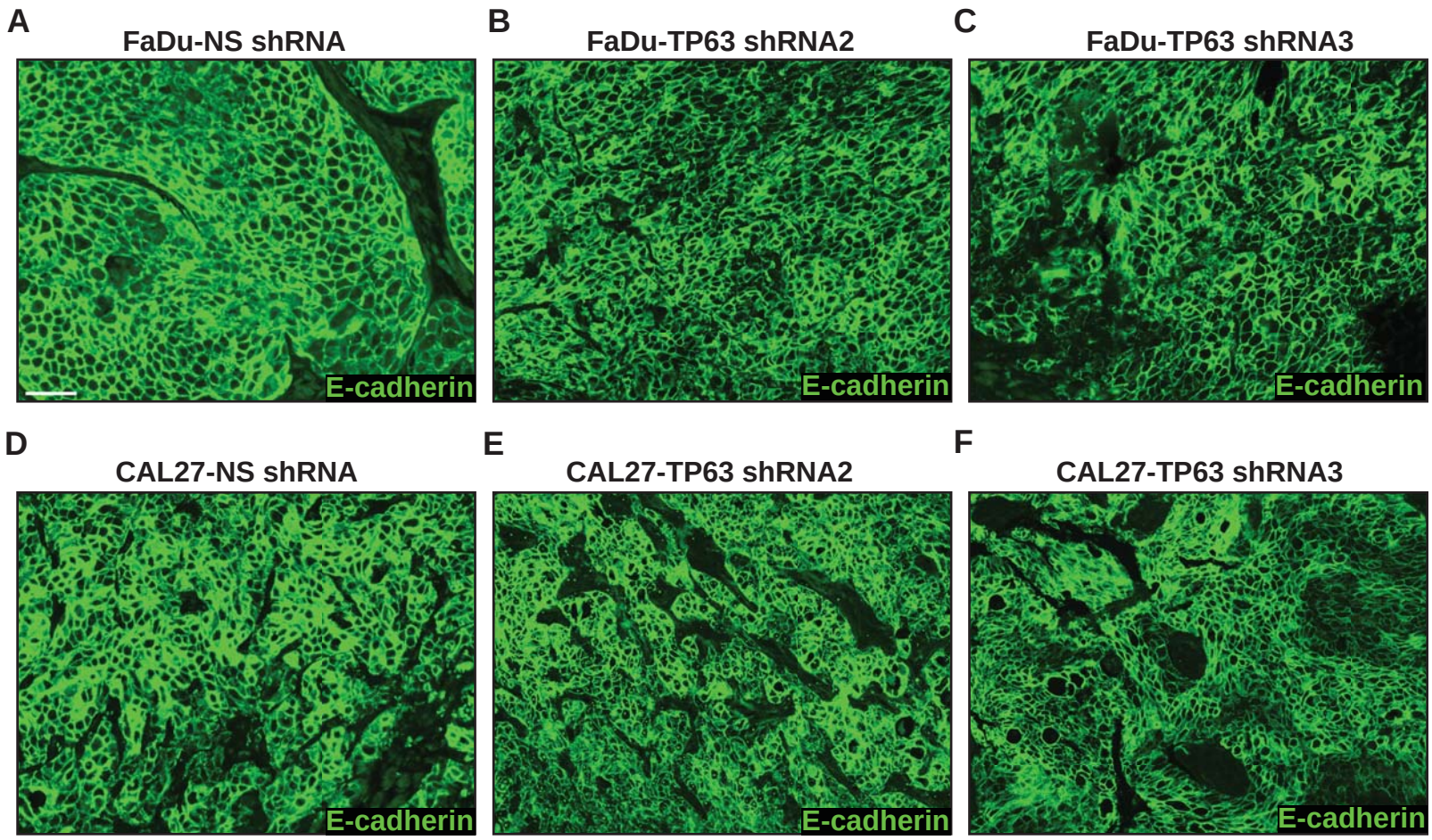

Supplementary Figure 8. Loss of TP63 in HNSCCs does not alter E-cadherin localization. (A-F) Immunostaining with antibody against E-cadherin on HNSCCs obtained by implanting athymic nude mice with FaDu-NS shRNA, FaDu-TP63 shRNAs (2 and 3), CAL27-NS shRNA, and CAL27-TP63 shRNAs (2 and 3) in to the tongue of athymic nude mice. Scale bars = 50 µm.

Supplementary Figure. 9

A

EGFR pathway

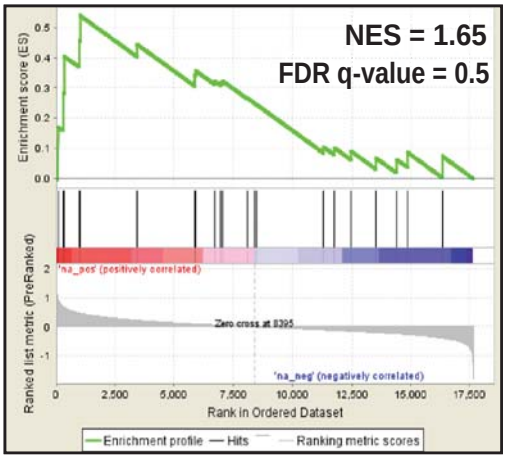

B

IL6-JAK-STAT3 pathway

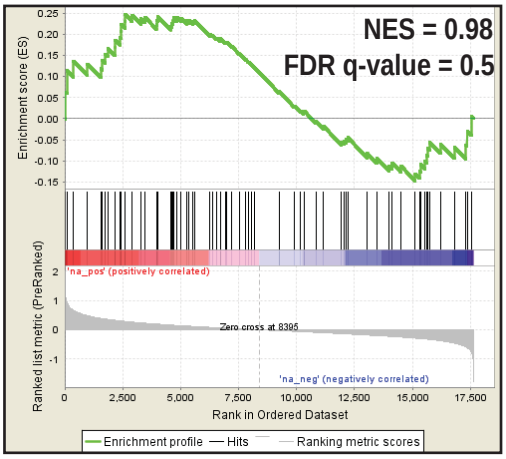

C

Enrichment plot: Biological_adhesion

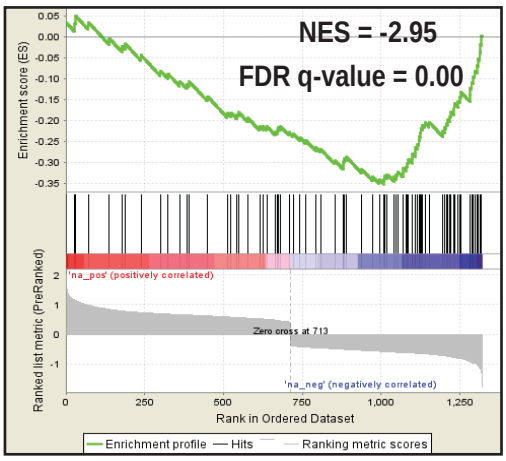

D

Category	Term	Count	P-value
GOTERM_BP_DIRECT	Negative regulation of cell proliferation	11	1.2×10^{-3}
GOTERM_BP_DIRECT	Bleb assembly	3	2.6×10^{-3}
GOTERM_BP_DIRECT	Positive regulation of cell migration	7	3.3×10^{-3}
GOTERM_BP_DIRECT	Positive regulation of cell proliferation	11	3.8×10^{-3}
GOTERM_BP_DIRECT	Hemidesmosome assembly	3	3.8×10^{-3}
GOTERM_BP_DIRECT	Epidermis development	5	4.5×10^{-3}
GOTERM_BP_DIRECT	Androgen metabolic process	3	6.8×10^{-3}
GOTERM_BP_DIRECT	Cytoskeletal organization	6	8.9×10^{-3}
GOTERM_BP_DIRECT	Ondotogenesis of dentin containing tooth	4	9.2×10^{-3}
GOTERM_BP_DIRECT	Signal transduction	18	9.5×10^{-3}
GOTERM_BP_DIRECT	Activation of MAPK activity	5	1.0×10^{-2}

Supplementary Figure 9. TP63 regulated pathways in HNSCCs identified using Gene Set Enrichment analysis (GSEA). (A, B and C) RNA-Sequencing on xenograft HNSCCs obtained by implanting athymic nude mice with FaDu-NS shRNA and FaDu-TP63 shRNA3 was performed as described under Methods. The differentially expressed genes in FaDu-TP63 shRNA3 HNSCCs (n=3) compared to FaDu-NS shRNA HNSCCs (n=3) were pre-ranked and the indicated pathways and (F) biological function were identified using GSEA. (D) Gene ontology (GO) term analysis using DAVID bioinformatic resources identified highly significant (P-value $\leq$ 0.01) biological processes regulated by TP63 in HNSCCs.

Supplementary Figure. 10

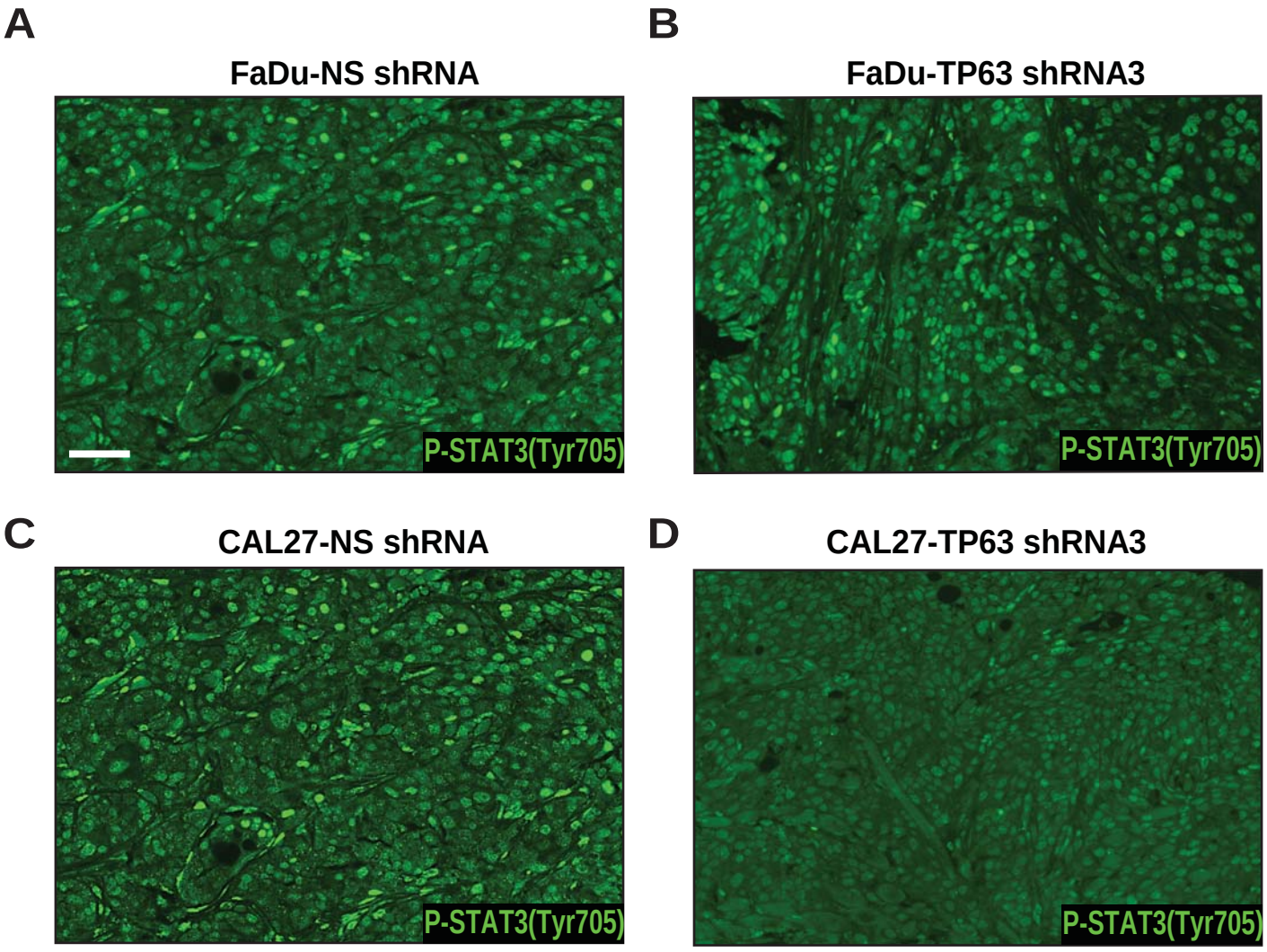

Supplementary Figure 10. Loss of TP63 in HNSCCs does not alter P-STAT3 (Tyr705) expression. (A-D) Immunostaining with antibody against P-STAT3 (Tyr 705) on HNSCCs obtained by implanting athymic nude mice with FaDu-NS shRNA, FaDu-TP63 shRNA3, CAL27-NS shRNA, CAL27-TP63 shRNA 3. Scale bars = 50 μm.

Supplementary Figure. 11

A

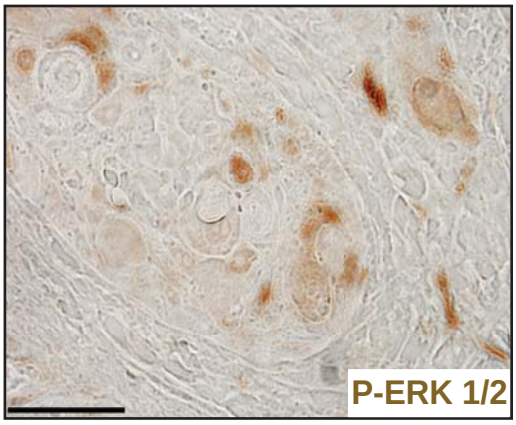

Well-differentiated larynx SCC

B

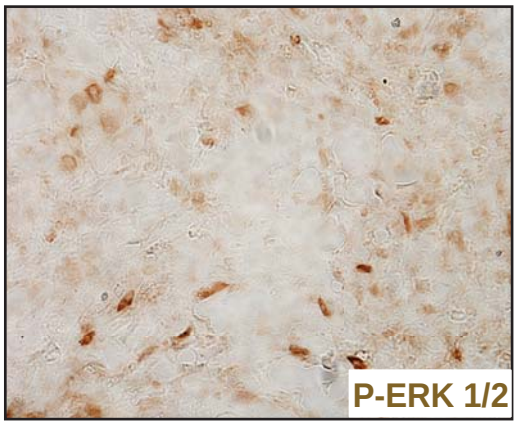

Poorly-differentiated larynx SCC

C

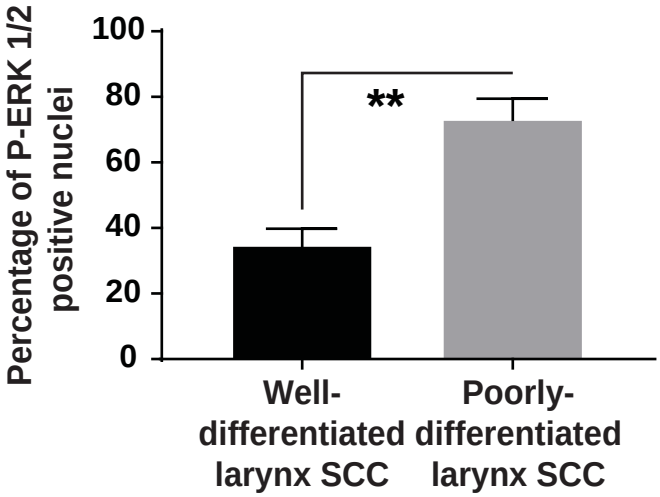

D

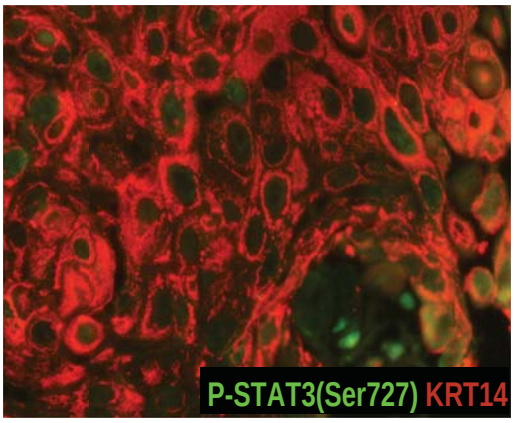

Well-differentiated larynx SCC

E

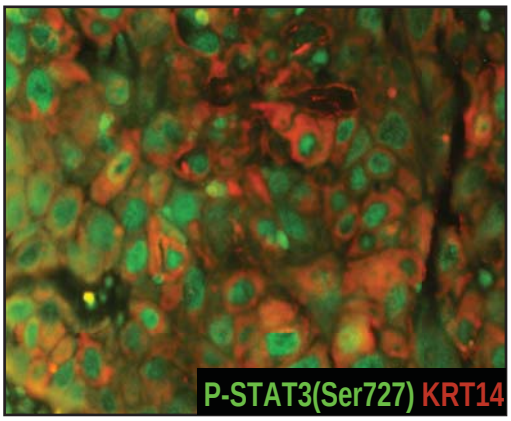

Poorly-differentiated larynx SCC

F

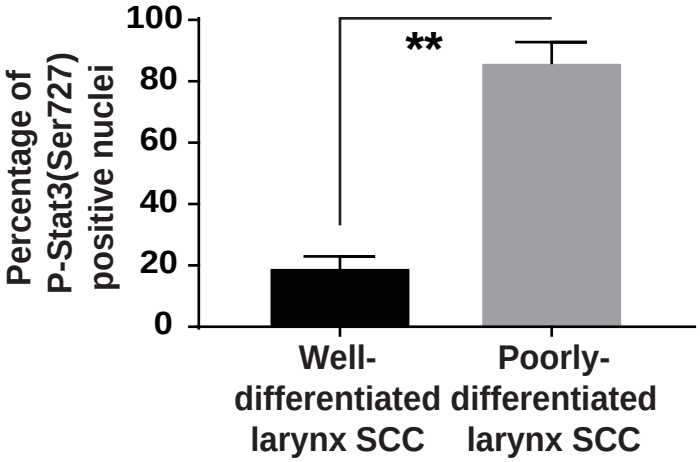

Supplementary Figure 11. MAPK and P-STA3 (Ser 727) signaling is upregulated in poorly-differentiated larynx SCCs. (A, B) Immunohistochemistry with an antibody against P-ERK1/2 (activated MAPK) on well- and poorly-differentiated larynx SCCs. Scale bars = 50 µm. (C) Quantification of P-ERK1/2 positive nuclei from A and B (two-tailed unpaired Student *t*-test, **: $P < 0.01$; Mean ± SD). (D, E) Immunostaining with an antibody against P-STAT3 (Ser727) on well- and poorly-differentiated larynx SCCs. (F) Quantification of P-STAT3 (Ser727) positive nuclei from D and E (two-tailed unpaired Student *t*-test, **: $P < 0.01$; Mean ± SD).

Supplementary Figure. 12

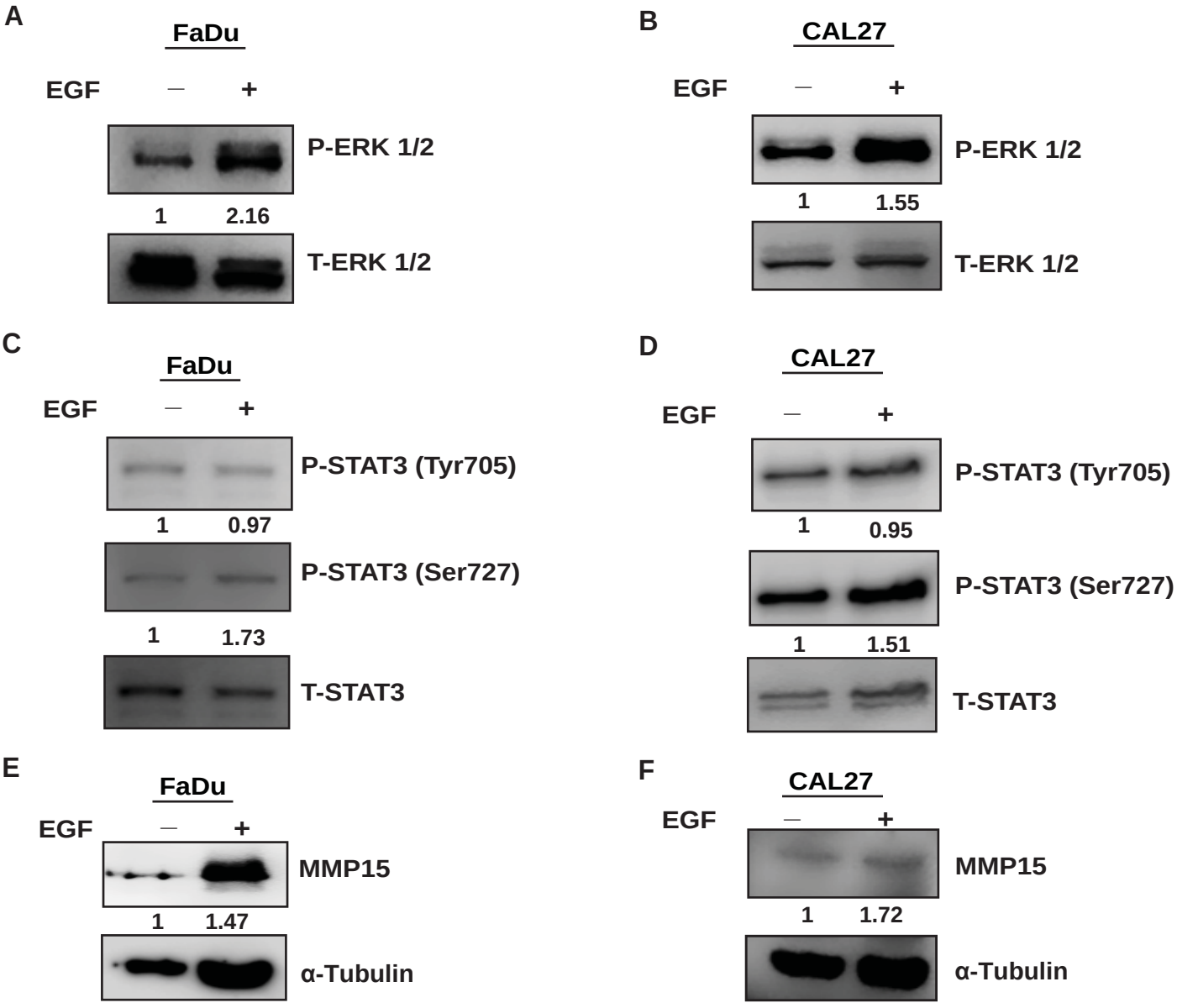

Supplementary Figure 12. EGF treatment of HNSCC cells leads to upregulation of P-ERK1/2, P-STAT3 (Ser 727), and MMP-15 in HNSCC cells. (A-F) FaDu and CAL27 cells were treated with EGF. P-ERK1/2, T-ERK1/2, P-STAT3 (Tyr705 and Ser727), T-STAT3, and MMP-15 protein levels in these cells were analyzed by western blotting. α-tubulin was used as loading control. Quantification of relative P-ERK1/2, P-STAT3 (Tyr705, Ser727) and MMP15 levels after normalizing to T-ERK1/2, T-STAT3, and β-actin is shown at the bottom.

Supplementary Figure. 13

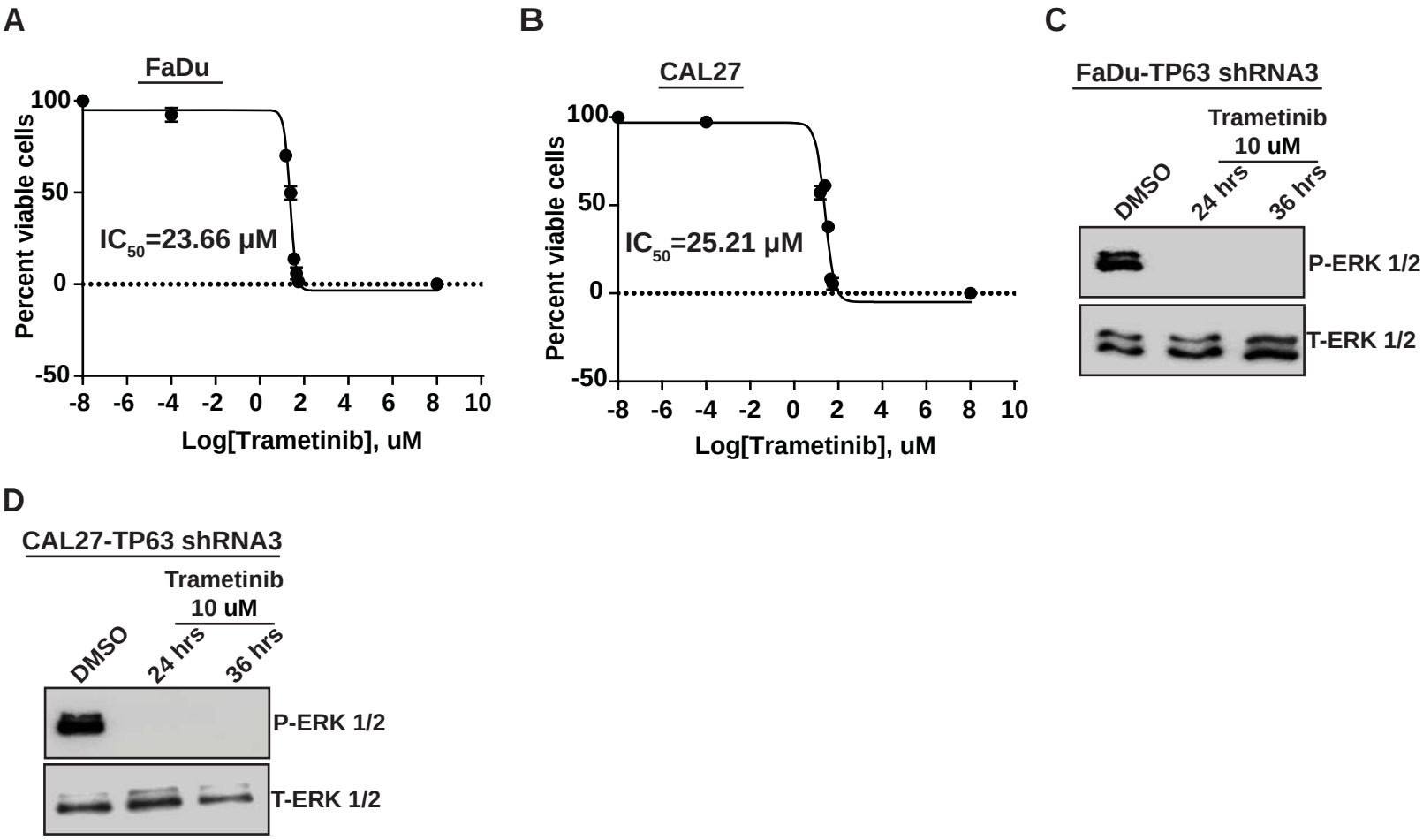

Supplementary Figure 13. Inhibition of MAPK signaling in HNSCC cell lines by treatment with Trametinib. (A, B) FaDu and CAL27 were treated with varying concentrations of Trametinib and IC50 was determined. (C, D) FaDu-TP63 shRNA3 and CAL27-TP63 shRNA3 were treated with either DMSO (vehicle) or 10 μM of Trametinib for 24 and 36 hours. P-ERK1/2 and T-ERK1/2 protein levels in these cells at indicated time points were analyzed by western blotting.

Supplementary Figure. 14

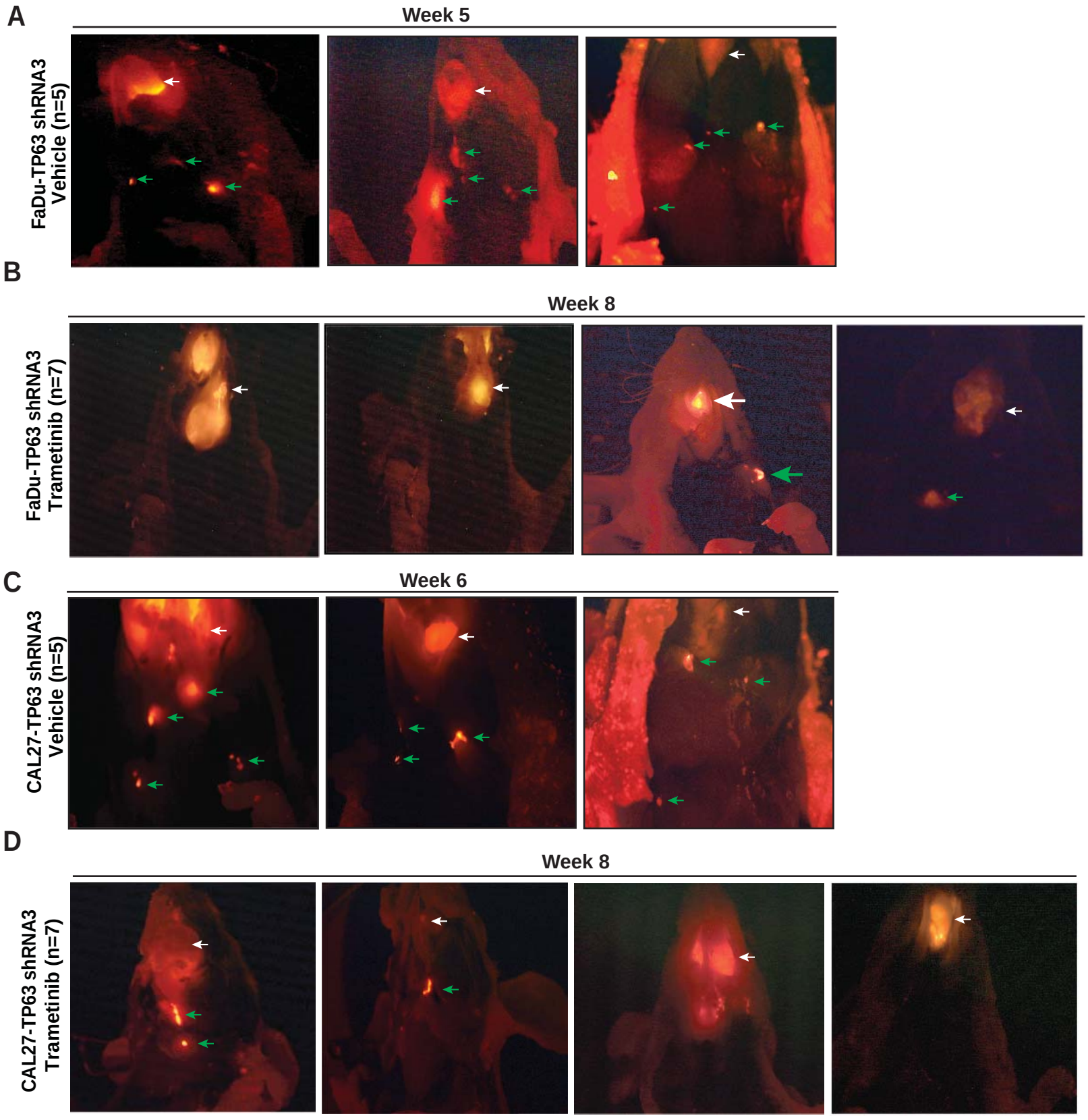

Supplementary Figure 14. Inhibition of MAPK signaling by Trametinib prevents the cervical lymph node metastasis of TP63 knockdown HNSCCs. (A-D) Athymic nude mice were implanted with FaDu-TP63 shRNA3 and CAL27-TP63 shRNA3 and treated with either vehicle or Trametinib. At the end of study, necropsy was performed, and HNSCCs were identified using fluorescence microscopy. Representative RFP images are shown. White arrows indicate primary tongue tumors and green arrows indicate metastatic tumors.

Supplementary Figure. 15

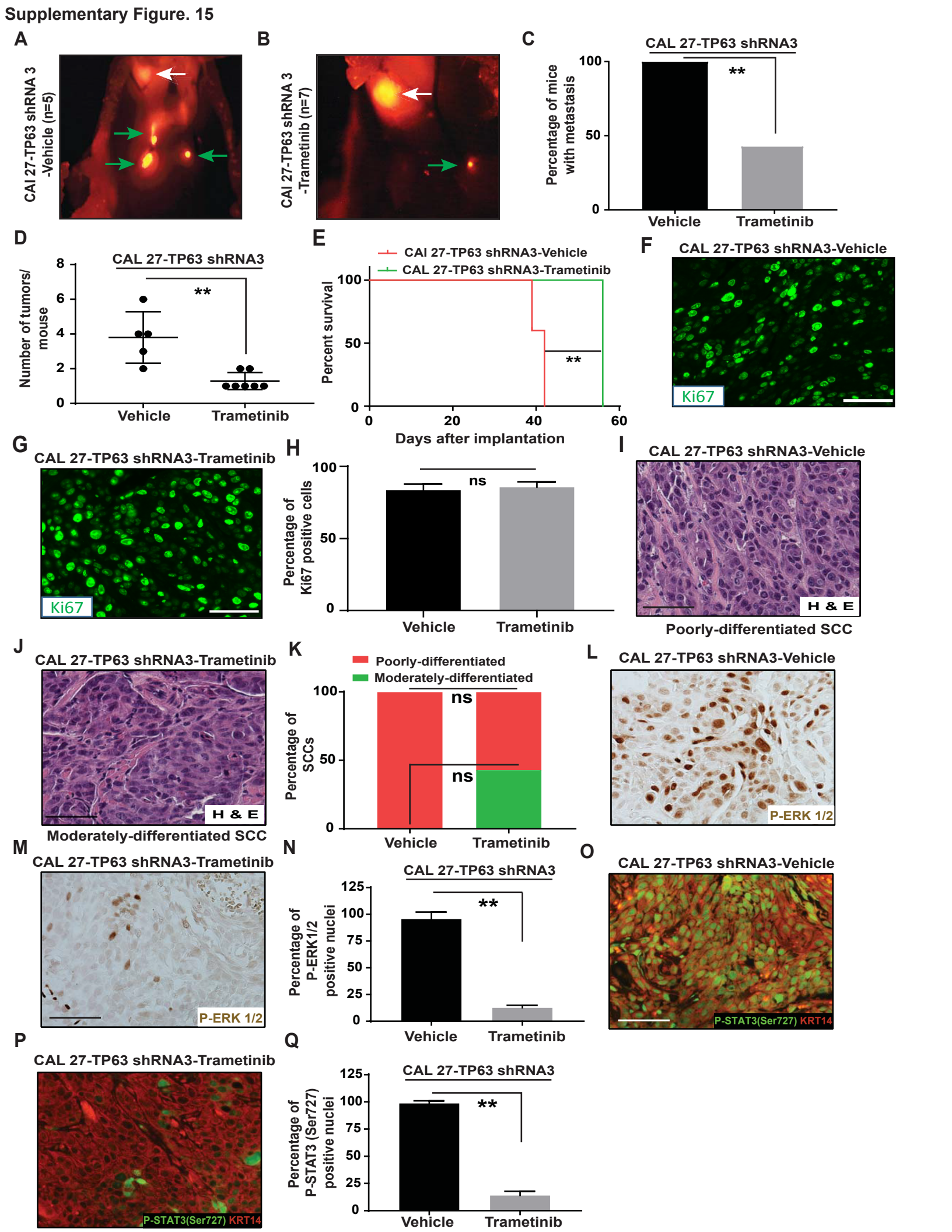

Supplementary Figure 15. Inhibition of MAPK signaling by Trametinib treatment prevents the cervical lymph node metastasis of CAL27-TP63 shRNA3 HNSCCs. (A, B) Athymic nude mice were implanted with CAL27-TP63 shRNA3 and treated with either vehicle or Trametinib. At the end of study, necropsy was performed, and HNSCCs were identified using fluorescence microscopy. Representative RFP images are shown. (C, D) Graphs depicting the percentage of mice with metastatic tumors (Fisher's exact test, **; $P < 0.05$) and average number of tumors/mouse (Mann-Whitney *U*-test, **: $P < 0.01$) in mice implanted with CAL27-TP63 shRNA3, and treated with either vehicle or Trametinib at the end of the study. (E) Graph depicting the survival (log-rank test, **: $P < 0.01$) of mice implanted with CAL27-TP63 shRNA3 and treated with either vehicle or Trametinib. (F, G) Immunostaining with antibody against Ki67 on SCCs obtained from mice implanted with CAL27-TP63 shRNA 3 cells and treated with either vehicle or Trametinib. (H) Quantification of Ki67 positive cells from F and G (two-tailed unpaired Student *t*-test, "ns" indicates not significant; $P > 0.05$). (I, J) Hematoxylin and eosin staining of moderately and poorly-differentiated HNSCCs obtained from mice implanted with CAL27-TP63 shRNA3 and treated with either Vehicle or Trametinib. (K) Graph depicting the percentage of moderately and poorly-differentiated HNSCCs obtained from I and J (Fisher's exact test, "ns" indicates not significant; $P= 0.06$). (L, M) Immunohistochemistry with antibody against P-ERK1/2 on HNSCCs obtained from mice implanted with CAL27-TP63 shRNA 3 and treated with either vehicle or Trametinib. (N) Quantification of P-ERK1/2 levels from L and M (two-tailed unpaired Student *t*-test, **: $P < 0.01$; Mean ± SD). (O, P) Immunostaining with an antibody against P-STAT3 (Ser727) on HNSCCs obtained from mice implanted with FaDu-TP63 shRNA 3 cells and treated with either vehicle or Trametinib. (Q) Quantification of P-STAT3 (Ser727) positive nuclei from O and P (two-tailed unpaired Student *t*-test, **: $P < 0.01$; Mean ± SD).